PAPER

Dynamics and chemical mode analysis of plasma thermal-chemical instability

To cite this article: Hongtao Zhong et al 2021 Plasma Sources Sci. Technol. 30 035002

View the article online for updates and enhancements.



IOP ebooks™

Bringing together innovative digital publishing with leading authors from the global scientific community.

Start exploring the collection-download the first chapter of every title for free.

Plasma Sources Sci. Technol. 30 (2021)035002 (16pp)

https://doi.org/10.1088/1361-6595/abde1c

Dynamics and chemical mode analysis of plasma thermal-chemical instability

Hongtao Zhong*

Mikhail N Shneider

ingqian Mao ,

and Yiguang Ju

Department of Mechanical and Aerospace Engineering, Princeton University, Princeton, NJ 08544, United States of America

E-mail: hongtaoz@princeton.edu

Received 31 October 2020, revised 9 December 2020 Accepted for publication 20 January 2021 Published 15 March 2021



Abstract

The stability of the weakly ionized plasma and the transition from a stable homogeneous discharge to unstable filaments play an important role in gas laser physics, plasma-assisted combustion, chemical reforming, and material synthesis. Theoretical stability analysis and thermal-chemical mode analysis were performed to understand the mechanism of plasma thermal-chemical instability by using a zero-dimensional plasma system with both simplified and detailed chemical kinetics of H₂/O₂/N₂ mixtures. The plasma dynamic and kinetic models accounted for multiple physical mechanisms in the chemically-reactive weakly ionized plasma, including ionization, attachment/detachment, recombination, vibrational and electronic energy relaxation, convective and diffusive species/heat removal, Joule heating, and detailed chemical kinetics. An analytical criterion and the explosive mode species/temperature pointers were formulated while the representative active species were identified for different thermal-chemical modes. The results showed that in addition to the classical thermal-ionization mechanism, various chemical modes from chemical heat imbalance and elementary kinetics significantly modified the time dynamics and the stability of the weakly ionized plasma. The present analysis provides insights and guidance to control plasma instability using chemical kinetics.

Keywords: plasma thermal-chemical instability, weakly ionized plasma, chemically-reactive flow, stability analysis, chemical mode analysis

Supplementary material for this article is available online

(Some figures may appear in colour only in the online journal)

Nomenclature

[]s Steady state quantities

 δ [] Perturbed quantities

[] Mixture-averaged quantities

[] Logarithmic normalized quantities

 $\beta_{\rm en}$ Electron-ion recombination coefficient, cm³ s⁻¹

 β_{ii} Ion–ion recombination coefficient, cm³ s⁻¹

g Source term in a general differential equation system

J Jacobian matrix of g

· Author to whom any correspondence should be addressed.

k Propagation constant, cm⁻¹

y N-dimensional column vector for a general differential equation system

 $\eta_{\rm T}$ Fraction of Joule heat responsible for direct heating

 $\eta_{\rm V}$ Fraction of Joule heat responsible for vibrational excitation

Y Mixture-averaged specific heat ratio

 $\cap \omega$ Vibrational quanta, eV

λ Eigenvalue of the Jacobian matrix, s⁻¹

Spatial operator for convection, drift and diffusion

O() At the order of

1

 μ_e Electron mobility, cm² V⁻¹ s⁻¹

 $\mu_{\rm n}$ Negative ion mobility, cm² V⁻¹ s⁻¹

```
\mu_{\rm p} Positive ion mobility, cm<sup>2</sup> V<sup>-1</sup> s<sup>-1</sup>
V_a Attachment rate, s<sup>-1</sup>
V<sub>d</sub> Detachment rate, s<sup>-1</sup>
V₁ Ionization rate, s⁻¹
V<sub>J</sub> Joule heating rate, s<sup>−1</sup>
V_{\beta} Electron-ion recombination rate, s<sup>-1</sup>
V_{\rm conv} Species/Heat removal rate, s<sup>-1</sup>
V_c Chemical heat releasing/absorption rate, s<sup>-1</sup>
\omega Cyclic frequency, 2\pi s<sup>-1</sup> \omega_i Total reaction rate of the species i, molecule cm<sup>-3</sup> s<sup>-1</sup>
\omega_{ij} Reaction rate of the species i in reaction j, molecule cm<sup>-3</sup>
s^{-1}
\Pi_{VV} Energy flow of vibrational quanta in the vibrational
domain, J cm<sup>-3</sup> s<sup>-1</sup>
\sigma Conductivity, \Omega^{-1} cm<sup>-1</sup>
T Convective/diffusive flow time scale, s
T VT Vibrational-translational (V-T) relaxation time scale,
= 1/v_{\rm VT}, s
c_p Specific heat, J K<sup>-1</sup>
E Electric field, V cm<sup>−1</sup>
E/N Reduced electric field, Td
E_{\rm v} Vibrational energy, eV cm<sup>-3</sup>
E_{\rm v}^0 Equilibrium vibrational energy, eV cm<sup>-3</sup>
f_iThermal-chemical mode corresponding to the eigenvalue \lambda_i
H Enthalpy of the mixture at gas temperature T_g, J mol<sup>-1</sup>
H_0 Enthalpy of the mixture at the ambient temperature T_0, J
h_i Enthalpy of the species i, J mol<sup>-1</sup>
I Current, mA
i_{\text{max}} Total species number
j_{\rm c} current density, mA cm<sup>-2</sup>
j_c E Joule heating, J cm<sup>-3</sup> s<sup>-1</sup>
j_{\text{max}} Total reaction number
k Boltzmann constant, J K<sup>-1</sup>
N Gas number density, cm<sup>-3</sup>
N_0 Ambient gas number density, cm<sup>-3</sup>
n_{\rm e} Electron number density, cm<sup>-3</sup>
N_i Gas number density of species i, cm<sup>-3</sup>
n_{\rm n} Negative ion number density, cm<sup>-3</sup>
n_{\rm p} Positive ion number density, cm<sup>-3</sup>
p Pressure, Torr
Q_c Chemical heat release/absorption, J cm<sup>-3</sup> s<sup>-1</sup>
Q_c^V Chemical heat release/absorption pumped into the vibra-
tional energy, J cm<sup>-3</sup> s<sup>-1</sup>
S Cross section of the plasma volume, cm<sup>2</sup>
T<sub>0</sub> Ambient gas temperature, K
T<sub>e</sub> Electron energy, eV
T<sub>g</sub> Gas translational temperature, K
T_{\rm v} Gas vibrational temperature, K
x_i Mole fraction of the species i
CSP Computational singular perturbation
NDCNegative differential conductivity
RAS Representative active species
SP Species/temperature pointer
```

TCM Thermal-chemical modes

1. Introduction

Weakly ionized gas plasma has been widely used in various plasma applications including high-energy gas lasers [1–4], geophysics [5, 6], plasma-assisted combustion [7–9], plasma-assisted chemical synthesis and material manufacturing [10–12]. The operating conditions are maintained by means of electric current flowing in a gas mixture under electric or electromagnetic fields. Heat/species diffusion/convection, volumetric energy transfer as well as the

chemical processes involving charged and excited particles formation and interactions all contribute to the rich dynamics

TCMA Thermal-chemical mode analysis

commonly-seen weakly ionized plasma states. In the former one, plasma is distributed uniformly within a large volume and resistant to perturbations. Energetic electrons, excited species and neutral species are in non-equilibrium. While in the latter one, inhomogeneous filaments are formed with much higher degrees of ionization and local gas temperature. Electrons and neutral species are closer to the equilibrium. The transition from the homogeneous non-equilibrium plasma discharge to filamentary near-equilibrium hot channels at sufficiently high energy inputs or enhanced pressures is critically important for its vast applications. To name a few, in molecular gas lasers (e.g. CO₂ and CO lasers), the transition from homogeneous states to contracted states will seriously erode the power capacity and optical quality of the active medium [2–4]. In plasmaassisted combustion, the homogeneous states will have prominent chemical effects and facilitate volumetric ignition due to its high electron energy, while the contracted states will have dominant thermal effects to force local ignition via its high gas temperature [13]. In plasma-assisted chemical manufacturing, thin filaments, formed through contraction of a diffuselike discharge, will have less efficiency and selectivity and may reduce the lifetime and chemical functionality of the catalysts. Moreover, from the viewpoint of fundamental research of plasma, the physical and chemical mechanisms behind the transition are also of interest. The contraction phenomenon provides one of the illustrative examples for the macroscopic self-organization of a gas plasma [14] as a consequence of mutual nonlinear influences of a variety of processes proceeding at a microscopic level. As such, there is a great need to perform stability and reaction kinetic analysis to better understand the criterion for transitions between the homogeneous and filamentary states involving plasma dynamics and elementary reactions and further optimize the performance of related devices.

The classical theoretical analysis for this homogeneous-filamentary-transition, known as 'plasma thermal instability', could be traced back to 1960–1980s [15–18]. The positive feedback of the thermal-ionization mechanism is expressed as,

$$T_{\rm g} \uparrow \rightarrow N \downarrow \rightarrow E/N \uparrow \rightarrow T_{\rm e} \uparrow \rightarrow V_{\rm i}(T_{\rm e}) \uparrow \rightarrow n_{\rm e} \uparrow \rightarrow j_{\rm c} E \uparrow \rightarrow T_{\rm g} \uparrow$$
.

From equation (1), at isobaric conditions, any local temperature rise will lower the gas number density (N) and further increase the reduced electric field (E/N). As a result,

(1)

the ionization rates controlled by E/N will increase. Faster ionization rates lead to higher production rates of electrons and more Joule heating. Later, more physical insights including the non-equilibrium electron distribution over velocities, ambipolar diffusion and the volumetric electron recombination were discussed in details for their influences on the transition [19]. Both experimental work [19] and numerical modeling [20, 21] for the contraction showed that the transition had a hysteresis cycle. Under some external discharge parameters, both homogeneous and contracted states could co-exist. By applying a sufficient perturbation, the homogeneous plasma could abruptly transform into a contracted state. However, previous studies of plasma thermal instability were mostly limited to noble gases, air [15, 18, 19, 21, 22] or mixtures in gas lasers [2-4]. How plasma instability would occur in chemically-reactive mixtures is not well understood.

Recently Zhong et al [23, 24] proposed a new concept of plasma thermal-chemical instability to address the positive feedback and couplings between plasma and plasma-enhanced chemical reactions in the reactive flow. With simulations of the dynamics of a self-sustained glow discharge in a reactive H₂ –O₂ –N₂ mixture, it was demonstrated that both the heat release/absorption and H₂ –O₂ chemical kinetics affected the critical plasma current for the transition between the homogeneous and the contracted states. This concept of plasma thermal-chemical instability has been validated in several experimental studies. Wolf et al [25] and Viegas et al [26] described the characteristic discharge modes in a CO₂ microwave plasma and showed the coupling between the

[26] described the characteristic discharge modes in a CO₂ microwave plasma and showed the coupling between the classical thermal-ionization instability and thermally-driven endothermic CO₂ dissociation reactions. Rousso *et al* [27] performed ICCD imaging and measured 1D time-resolved *in situ* electric field in a nanosecond pulsed dielectric barrier discharge plasma of O₂—Ar mixtures with and without CH₄ (fuel) addition. They found that the rapid formation of streamers from an originally uniform discharge appeared to be caused by the chemical kinetics of plasma-assisted low temperature CH₄ oxidation. These results again highlighted the impact of chemical kinetics on the contraction phenomena of reactive

molecular gas plasmas. However, how such a thermalchemical instability initiates and how the character of the governing differential equations transit from one stable homogeneous solutions into another unstable filamentary solutions in accordance with not only discharge parameters but also chemical kinetics parameters are not understood well. In addition, it is not clear which reactions or species contribute to what extent to the growth of the unstable modes of the plasma instability.

Transitions and critical conditions for the weakly ionized plasma have been discussed for decades [1, 16, 28]. Mathematically, it is equivalent to the stability analysis of a system of differential equations consisting of species/energy balance equations as

$$\frac{\partial \mathbf{y}}{\partial t} + \mathsf{L}(\mathbf{y}) = \mathbf{g}(\mathbf{y}). \tag{2}$$

The unknowns in the target system are denoted as an N-dimensional column vector \mathbf{y} as a function of time and spatial variables. \mathbf{g} is the source term and $\mathbf{L}(\mathbf{y})$ is the spatial operator for convection, drift and diffusion. The system can

be linearized by substituting expressions as $\mathbf{y} = \mathbf{y}_0 + \delta \mathbf{y}$ for unknowns and assuming that the perturbations $\delta \mathbf{y}$ are small. The solution of the linearized system is sought in the form of plane waves as $\delta \mathbf{y} = \mathbf{y}_0 e^{\mathrm{i}(\mathbf{k} \cdot \mathbf{x} - \omega t)}$, which yields a system of n algebraic equations involving steady-state values \mathbf{y}_0 . Setting the determinant of the system to zero yields the dispersion relations involving propagation constant \mathbf{k} , frequency $\boldsymbol{\omega}$ and other physical parameters as

$$D(\boldsymbol{\omega}, \mathbf{k}) = 0. \tag{3}$$

If at least one of the n complex roots satisfies $\text{Im}(\omega) > 0$ at a given **k**, perturbations will grow exponentially. The crit-ical condition for the system to become linearly unstable corresponds to

$$\max[\operatorname{Im}(\boldsymbol{\omega}(\mathbf{k}))] = 0 \tag{4}$$

which physically represents the transition between contracted (unstable, $\max[\operatorname{Im}(\omega)] > 0$) and homogeneous (stable, $\max[\operatorname{Im}(\omega)] < 0$) plasma states. Under the zero-dimensional assumption ((y) = 0, k = 0), the above analysis is equivalent to compute the eigenvalues λ of the Jacobian matrix of the source term g, defined as

$$\mathbf{J} = \frac{\partial \mathbf{g}}{\partial \mathbf{y}}.$$
 (5)

The conversion between λ and ω is $\lambda = i\omega$. Then equation (4) is equivalent to

$$\max[\operatorname{Re}(\lambda)] = 0. \tag{6}$$

For the consistency with previous analysis on chemical modes [29, 30], we stick to the notation of equation (6) for the critical conditions in the following content. However, the methodology is mathematically equivalent with equation (4) and previous analysis on plasma waves and instabilities [1, 28]. For simplified systems with a reduced number of species, the critical conditions can be derived by hand to gain the physical and chemical insights. For realistic systems with detailed chemistry, such dependence of the stability on the species and reactions is often computed numerically using numerical perturbation. By inspection of the numerical data, reaction modes and sensitivity of individual reactions and species towards the plasma thermal-chemical instability can be further discussed [29].

The objective of this work is to analyze the stability of weakly ionized plasma in the presence of chemical kinetics to gain insights on the control of plasma thermal-chemical instability. The paper is structured as the following: in section 2, both a general formulation with detailed chemistry and a self-consistent model with simplified chemistry are provided to describe the dynamics of the thermal-chemical instability for reactive plasmas and the foundations for the stability analysis are laid. In section 3, the stability criterion and chemical modes of such a reacting system are derived analytically under simplified kinetics or computed numerically under detailed kinetics. The explosive modes and their 'representative active species' (RAS) associated with elementary kinetics for plasma thermal-chemical instability are presented. The influence

of different physical-chemical mechanisms including heat addition/absorption, vibrational-translation relaxation, attachment/detachment and elementary kinetics on the stability of a reactive plasma system is investigated. Finally, conclusions and future work are provided in section 4.

2 Zero-dimensional plasma model

The transitions from homogeneous to filamentary plasma states have been demonstrated in different low temperature plasma power sources [13, 20, 25, 27]. To simplify the plasma kinetic modeling and remain the generality of the plasma thermal-chemical instability, the discussion below is limited to a DC glow discharge in the mixture of molecular gases. The extension of such analysis to other discharges can be done in a similar way. These plasmas in the positive column of the glow discharge are characterized by pressures of 10–300 Torr, relatively low electron energy (~1 eV), and low ionization degree (below 10^{-6}). The general behavior of such a plasma is governed by an exceedingly complex network of energy transfer and chemical interactions [16] and requires an extensive multidimensional description. Nevertheless, previous numerical simulations [2, 16, 31] have shown that to determine the dominant mechanisms corresponding to a particular circumstance, assumptions should be made which match related time scales, retain essential physical features while greatly reducing the complexity of the analysis.

On the basis of such considerations, we assume that the instability grows from the initially homogeneous plasma. Under those assumptions, we simplify the problem as zero-dimensional. This zero-dimensional assumption will be further examined in section 3.4 and validated with previous one-dimensional results [20, 21, 23, 24]. A demonstration figure of zero-dimensional stability analysis is shown in figure 1, where we consider $H_2 - O_2 - N_2$ chemistry and separate the contracted states and the homogeneous states by their different gas temperatures, discharge power inputs and active species. In this section, a general formulation for detailed kinetics and a simplified model with reduced kinetics for the zero-dimensional plasma system will be presented. In addition, the methodology for analytical/numerical perturbation will also be introduced briefly.

21. A general zero-dimensional formulation

The general zero-dimensional formulation consists of a system of ordinary differential equations for species and temperature as

$$\frac{\mathrm{d}N_i}{\mathrm{d}t} = \int_{j=1}^{j_{\text{max}}} \omega_j(t) - \frac{N_i}{\tau} \quad (i = 1, 2, 3, \dots, i_{\text{max}})$$
 (7)

$$\frac{Y}{V} k \frac{\mathrm{d}(NT_{\mathrm{g}})}{\mathrm{d}t} = j_{\mathrm{c}}E - \frac{3}{2} k \frac{\mathrm{d}(n_{\mathrm{e}}T_{\mathrm{c}})}{\mathrm{d}t} - \frac{i_{\mathrm{max}}N_{i}}{h_{i}} - \frac{H - H_{0}}{\mathrm{d}t},$$

$$Y - 1 \quad \mathrm{d}t \qquad 2 \quad \mathrm{d}t \qquad dt \qquad T$$

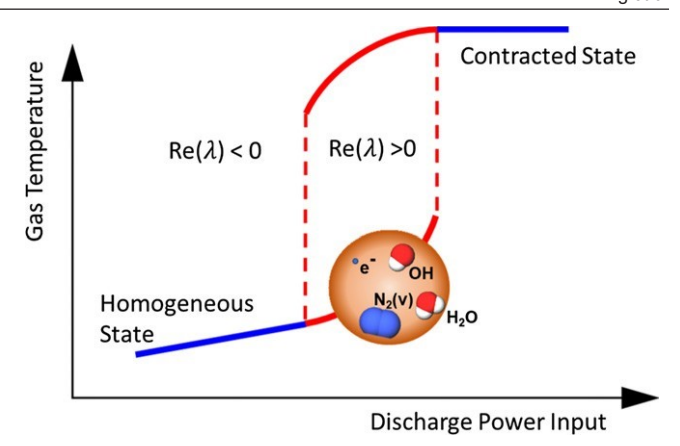


Figure 1. The schematic of zero-dimensional stability analysis of plasma thermal-chemical instability in the H_2 – O_2 – N_2 system. Under low plasma current, the homogeneous plasma volume remain stable (shown as the blue lower branch). With increased energy input (above some criticality), perturbations through the plasma system will self-amplify and rich kinetics and dynamics are expected (shown as the transition region in red). Eventually the system will transit to the contracted state (shown as the upper branch) through non-equilibrium energy transfer and plasma-assisted chemical pathways.

where *i* is the species index in the chemical mechanism and N_i is the number density of species i. ω_{ij} is production or consumption rate of species i contributed by reaction j. i_{max} and j_{max} are the total numbers of species and reactions in the chemical mechanism. T is the characteristic time for the effective removal of charged particles and energy by convection and diffusion transport. It is frequently used in theoretical studies to make the zero-dimensional calculations more tractable. The formulation of gas translational temperature $T_{\rm g}$ is similar with Flitti and Pancheshnyi's method [32]. The total electric power ($j_e E$) is distributed into four parts: the translational degree of freedom of electrons, the translational degree of freedom of gas, the internal degree of freedom of gas and the convective loss. y is the mixture-averaged specific heat ratio and h_i is the specific enthalpy of species i. H is the enthalpy of the mixture at the temperature T_g while H_0 is the enthalpy of the same mixture at the ambient temperature T_0 . The current density j_c in the total electric power term is defined as $j_c = e(\mu_e n_e + \mu_n n_n + \mu_p n_p)E$. The chemical mechanism following this formulation should include relevant reactions such as electron-impact reactions (excitation, dissociation, attachment and ionization), quenching/relaxation reactions of vibrationally/electronically excited states, charged species interactions (detachment, charge exchange, electron-ion and ion-ion recombination) and elementary chemical kinetics of

molecules and radicals. The gas heating from all the abovementioned reactions is considered for the time evolution of the gas translational temperature.

Two auxiliary relations are used to couple the whole system. One relates external current, conductivity and electric field as

(8)
$$\underline{\qquad} E(t) = \frac{I}{\sigma(t)S}$$

(9)

Here the discharge current, I, determined by the external electric circuit and defined as a parameter, can be related with electric field E(t), conductivity $\sigma(t)$, which is calculated as $e(\mu_e n_e + \mu_n n_n + \mu_p n_p)$, and characteristic cross section of the zero-dimensional plasma volume S. The other is the ideal gas

assumption as

$$p = \sum_{i} N_i \ kT_{\rm g},\tag{10}$$

where $\Sigma_i N_i$ is a summation of the neutral and ion species. The contribution from electrons is neglected as $n_e \Sigma_i N_i$ is sat- isfied in the weakly ionized plasma. The discussion is further limited to isobaric conditions. Equations (7)–(10) form a gen-

eral zero-dimensional formulation for the thermal-chemical instability, consistent with previous investigations in plasma assisted ignition and plasma-combustion kinetic studies [33].

The above formulations are implemented numerically in

this work. The plasma chemistry library ZDPlasKin [34] and

the chemical kinetics library CHEMKIN [35] are integrated using a time-splitting numerical scheme [33, 36, 37]. The electron energy distribution function (EEDF) and the rate coefficients of electron-impact reactions are calculated by a Boltz-

mann equation library BOLSIG+ [38]. The cross sections of electron-impact reactions are obtained from the LXCat Project [39] and more details are provided in supplementary mate- rial (https://stacks.iop.org/PSST/30/035002/mmedia). For the demonstrative example as the plasma thermal-chemical instability in the $H_2 - N_2 - O_2$ mixture in section 3, the chemical mechanism includes 62 species, 151 elementary reactions and 666 plasma reactions. 69 electron-impact reactions are considered for the EEDF calculation. This $H_2 - O_2 - N_2$ combustion mechanism is developed from Princeton HP-MECH [40]. The sub-mechanism of NOx is from [37]. Excited and charged species in the mechanism include $N_2(v)(v = 1-8)$, $H_2(v)(v = 1-3)$, $O_2(v)(v = 1-4)$, $O_2(b^1\Sigma^+)$, $O_3(b^2\Sigma^+)$, O_3

$$O^+, O^+, H_3O^+, O^-, O^-, O^-, O^-$$
, OH- and electron. The gas heat-

ing from reactions involving N₂, O₂ [32], H₂ [41] and related radicals and plasma species are all considered. The corresponding detailed reactions are provided in the supplementary material.

22 A simplified zero-dimensional model

The above general formulations enable detailed modeling of the dynamics of the thermal-chemical instability for realistic reactive plasmas. However, complicated chemical kinetics may hinder the analytical study of the stability boundary and obscure valuable physical insights for the zero-dimensional plasma system. Therefore, a simplified zero-dimensional model with five independent variables is pre-sented. This simplified model is consistent with our general formulation in section 2.1 given the same chemical mechanism (details are provided in the supplementary material) and more importantly,

temperature equations (T_g) as

$$\frac{\mathrm{d}n_{\mathrm{e}}}{\mathrm{d}t} = \overline{\nu}_{\mathrm{i}}n_{\mathrm{e}} - \overline{\nu}_{\mathrm{a}}n_{\mathrm{e}} + \overline{\nu}_{\mathrm{d}}n_{\mathrm{n}} - \overline{\beta}_{\mathrm{ep}}n_{\mathrm{e}}n_{\mathrm{p}} - n_{\mathrm{e}}/\tau \tag{11}$$

$$\underline{dn}_{n} = \overline{V} n - \overline{V} n - \overline{\beta} n n - n / T$$

$$dt \qquad a \quad e \quad d \quad n \quad \text{ii} \quad n \quad p \quad n$$

$$(12)$$

$$\frac{dn_{\rm p}}{dt} = \overline{\nu}_{\rm i} n_{\rm e} - n_{\rm p} / \tau - \overline{\beta}_{\rm ep} n_{\rm e} n_{\rm p} - \overline{\beta}_{\rm ii} n_{\rm n} n_{\rm p} - n_{\rm p} / \tau \qquad (13)$$

$$N\overline{c}_{p} \frac{dT_{g}}{dt} = \eta_{T} j_{c} E + \Pi_{VV} + \frac{E_{v} - E_{v}^{0}}{\overline{\tau}_{VT}} + Q - N \overline{\epsilon} \frac{T_{g} - T_{0}}{\tau}$$
(14)

$$\frac{dE_{v}}{dt} = \eta_{v} j_{c} E - \Pi_{VV} - \underline{E} - \underline{E}^{0} + Q^{V}$$

$$\frac{\overline{\tau}_{VT}}{-(N_{0}/N) \frac{E_{v} - E_{v}^{0}}{\tau}} \cdot . (15)$$

One must note that the number of independent variables in the simplified system can be increased, if needed. In addition, in the reactive flow, plasma kinetic parameters including ionization, attachment and detachment frequencies are all functions of the composition x_i . The notation $[\]$ is used to denote all mixture-averaged quantities in the simplified model. From equations (11)–(13), charged species are controlled by ionization, attachment/detachment, electron—ion/ion—ion recombination processes and convective removal. In the gas temperature equation [equation (14)], terms on the right-hand side represent Joule heating, energy flow of vibrational quanta in the vibrational energy domain, V–T energy relaxation, convective heat removal and the energy exchange from chemical kinetics of neutral species, denoted as Q_c . For

excited plasma kinetics, only the vibrational excitation, V-V

it lays foundations for the analytical investigation of the stability criterion in the next section.

The zero-dimensional simplified system is composed of charged species continuity (electron number density n_e , negative ion number density n_n , positive ion number density n_p) and energy equation (vibrational energy (E_v) and translational

(1 eV). The vibrational energy E_v is assumed to store inone vibrational level of the diluent (e.g. N_2) for simplification and is linked with the vibrational gas temperature T_v as $E_V = N \cap \omega / \exp n\omega / kT_V + 1$. On the right-hand side of equation (15), the term Q^V is also included, which represents the heat release or absorption of the vibrational energy from reactions such as

$$N_2(v = 1) + H_2 \longrightarrow N_2 + H_2$$
 (R1)
 $N_2(v = 1) + H_2O \longrightarrow N_2 + H_2O.$ (R2)

EEDF is not solved in this simplified system. Instead BOLSIG+ is applied in advance to generate a check-up table for $T_e(E/N)$ relations to link reduced electric field to kinetic coefficients.

23 Perturbation analysis

The linear stability analysis starts from small wave-like departures (denoted as $\delta[]$) from the equilibrium values (denoted as

[]_s) of the major variables. Here, perturbations of several key quantities for the plasma thermal-chemical instability are presented. First, a perturbation of the current–voltage relation in equation (9) yields

$$\frac{\delta E}{E_{\rm s}} + \frac{\delta \sigma}{\sigma_{\rm s}} - \frac{\delta I}{I} = 0. \tag{16}$$

According to equation (1), when the ionization is intensified, more electrons are accumulated and the conductivity builds up exponentially ($\delta\sigma > 0$), leading to a drop in the electric field ($\delta E < 0$) given the current is unchanged. The fluctuations from the electric field and the conductivity can further spread to the Joule heating term in the temperature equation as

$$\delta(jE) = (jE) \frac{\delta\sigma}{} + 2\frac{\delta E}{} . \tag{17}$$

$$c c s \sigma_{s} E_{s}$$

From the expression, $\delta(j_c E)$ is controlled by the growth of the electron number density and hence the conductivity as well as the dropping of electric field.

Another key quantity for controlling the plasma kinetics is the reduced electric field (E/N). The perturbed reduced electric field E/N could be written as

$$\delta \quad \frac{E}{N} = \frac{E}{N} \frac{\delta T}{s} \frac{\delta E}{T_s} . \tag{18}$$

Clearly two physical processes contribute to the fluctuation of E/N. One is the temperature perturbation or thermal expansion. Positive temperature perturbation ($\delta T > 0$) induces positive increment of reduced electric field ($\delta(\frac{E}{N}) > 0$). The other is the charge accumulation or the electric field drop. High steady-

state electric field (E_s) or temperature (T_s) may inhibit the growth of the reduced electric field. The perturbation will fur-

ther propagate from the reduced electric field to plasma kinetic processes as E/N controls the EEDF and critical processes like ionization, attachment/detachment and recombination.

The perturbed N-dimensional column vector δy forms a linearized ordinary differential equation system. The linear stability analysis is converted into calculating matrix eigenvalues of this dynamical system. The stability boundary in the parameter space is determined by equation (4) and presented in section 3. For simplified plasma reaction systems, the steady-state stability boundary is derived analytically and the results are validated numerically by using the MATLAB symbolic toolbox.

24. Thermal-chemical mode analysis

To better characterize the thermal-chemical instability and understand how the thermal-chemical modes and the stability behavior evolve with respect to time, for detailed plasma reaction systems, we follow the computational singular perturbation theory [29, 30] and develop the thermal-chemical mode

decomposition of the Jacobian matrix [defined in equation (5)] at different time moments as

$$\frac{\mathrm{d}}{\mathrm{d}t}\delta\mathbf{y} = \mathbf{J} \cdot \delta\mathbf{y} = A\Lambda B \cdot \delta\mathbf{y}.\tag{19}$$

 Λ is the diagonal matrix as diag($\lambda_1, \lambda_2, \ldots, \lambda_N$). A and B are composed of column and row eigenvectors, respectively. This Jacobian matrix consists of thermal-chemical property for the system and defines thermal-chemical 'modes' (TCM) in the system as

$$\frac{\mathrm{d}}{\mathrm{d}t}f_i = \lambda_i f_i, \quad f_i = B \cdot \delta \mathbf{y}, \quad i = 1, 2, \dots, N.$$
 (20)

Eigenvalues of the Jacobian with positive real parts (Re(λ_i) > 0) indicate that the system is unstable or 'explosive'. The associated chemical modes tend to grow exponentially with the time scale of λ_i^{-1} . If no positive eigenvalues are

present, the system is linearly resistant to perturbations and approaching the chemical equilibrium as all chemical modes tend to decay. Thus, the zero-crossing of an eigenvalue from negative to positive is the critical condition for the stability of the system [equation (6)].

To understand which species and reactions are contributing to the explosive TCMs and to further project the system stability to the species space, the concept of 'explosive mode

species/temperature pointer' (SP) is defined, which is similar to the 'radical pointer' used in previous combustion kinetic studies [29, 30] as

$$SP_i = diag(\mathbf{a_i} \cdot \mathbf{b_i}) \quad i = 1, 2, \dots, N, \tag{21}$$

where $\mathbf{a_i}$ and $\mathbf{b_i}$ are the right and left eigenvectors, respectively, associated with λ_i and the chemical mode f_i . The kth entry of SP_i indicates the correlations between the kth variable in the column vector \mathbf{y} and the ith chemical mode f. The 'RAS' for

the chemical mode f_i is defined as the species which has the

analysis (TCMA) to analyze the stability and chemical modes of the zero-dimensional plasma system with chemical kinet- ics (detailed numerical implementation is introduced in supplementary material). The analysis is based on the eigenvalue

3. Results and discussions

Given the above formulations, we perform perturbations around the steady states (sections 3.1, 3.2 and 3.4) or mode analysis at discrete times (section 3.3) and discuss the stability criterion or the transition caused by the thermal-chemical effects in a zero-dimensional plasma system. Specifically, eigenvalues and eigenmodes ($\text{Re}(\lambda)$) are provided both at steady states or during the time evolution to consider the influence from chemical kinetics.

The N_2 – O_2 and H_2 – O_2 – N_2 mixtures are mainly discussed for several reasons. First, hydrogen is a clean efficient energy carrier and widely used in plasma assisted chemical synthesis while air is the most convenient bath gas. Second, rich chemical kinetics of the H_2 – O_2 – N_2 mixture and possible formations of O_3 , NO_x , H_2O and NH_3 have been reported previously [41, 42]. Potential couplings between the thermal-ionization mechanism and chemical kinetics are expected in this mixture. Surely the plasma thermal-chemical instability is universal and not limited to some certain species. Nevertheless, discussions of other reacting systems are beyond the scope of the this work.

The mixture is set in a preheated environment (400–800 K) for elevated chemical reactivity (consistent with previous discussions on 'warm' plasmas [43]). The pressures are varied from 50-250 Torr while convective time scales are varied from 1 ms-10 ms. Those values are adjusted to keep the critical current in a reasonable range (1–100 mA).

31. Eigenmodes of endothermic/exothermic reactions

The thermal effect has been discussed in the classical thermalionization mechanism [22] by only perturbing the gas translational energy equation [equation (14)] with negligible energy transfer from the vibrational energy (\mathbf{Q}_T 1, $\Pi_{VV \geq 0}$). The eigenmode under those simplifications is

Re()
$$\sigma_{\rm s}E^2$$
 $\frac{\partial \ln n_{\rm e.s}}{\partial \ln T_{\rm s}}$ $\frac{1}{\tau}$ $\frac{\partial \hat{v}_{\rm i}}{\partial \hat{v}_{\rm conv}}$, $\frac{\hat{E}}{\partial \hat{v}_{\rm conv}}$, (22)

where V_J $\sigma_s \frac{\sigma_s E^2}{N_0 c_p T_0}$ is the Joule heating rate, V conv is the heat $=\frac{s}{s}$ removal rate, while $\frac{\partial V_1}{\partial (\widehat{N})}$ is the normalized sensitivity of

the ionization frequency towards the reduced electric field. Equation (22) demonstrates the stabilization of heat removal and the destabilization by Joule heating and ionization. However, the influence of endothermic/exothermic reactions is neglected. A straightforward extension by considering chemical heat absorption/release term Q_c in equation (14) yields

Re()
$$\approx V_{\rm J} - \frac{\partial \hat{V}_{\rm i}}{\partial \hat{E}} - V_{\rm conv} + V_{\rm c}.$$
 (23)

Clearly there is an additional exothermicity term as V_c =

 $\frac{1}{N_0} \frac{\partial Q_c}{\partial r}$ besides the nonlinear 'ionization-avalanche' term in

the eigenmode now and the system could be stabilized or destabilized depending on the sign of it.

A more detailed stability analysis includes the electron number density [equation (11)] and gas translation temperature [equation (14)]. By including only two equations, electronegative species are excluded $(n_{\approx}n_{\rm p})$ and energy transfer from vibrational energy is negligible (which is reasonable at relatively low gas temperature, see discussions in section 3.2). The characteristic equation is updated to

$$\lambda^{2} + \lambda(-v_{c} + v_{conv} + v_{\beta}) + v_{\beta}v_{conv} - v_{\beta}v_{c} - \frac{\frac{\partial v}{\partial v_{conv}}}{\frac{1}{\partial v_{conv}}} v_{J}v_{i} = 0$$

 V_{β} is defined as electron—ion recombination rate $\beta_{\rm ep} n_{\rm e,s}$. The stability boundary could be written as

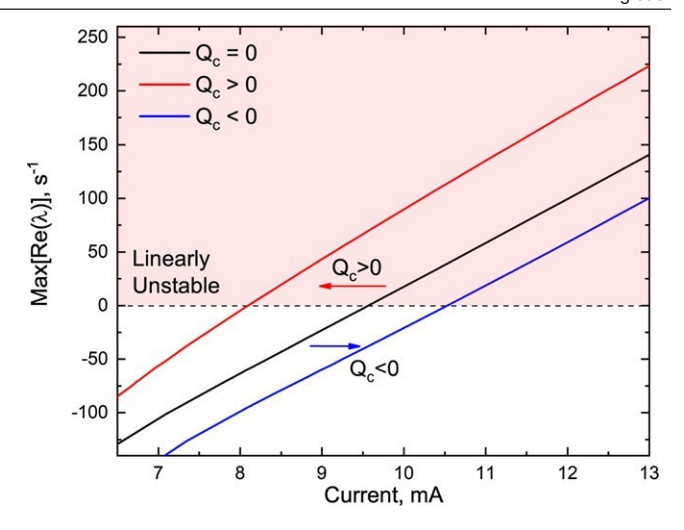


Figure 2. p = 105 Torr, $T_0 = 600$ K. $Q_c = 0$ refers to a $N_2 - O_2$ mixture without any influence from endothermic/exothermic

reactions. $Q_c > 0$ refers to the $N_2 - O_2$ mixture with influence from exothermic reactions. $Q_c < 0$ refers to the $N_2 - O_2$ mixture with

influence from endothermic reactions.

Table 1. The comparison of exothermic and endothermic reactions. Current I = 9.5 mA. The mixture is $N_2 - O_2$ at $T_0 = 600$ K and p = 105 Torr. Convective time scale $\tau = 1$ ms. $\tau \frac{\partial Qc}{\partial T}$ is the chemical heat release/absorption normalized by the heat convection term. (Vine)* is the normalized ionization term, defined as $(V n) = \frac{V_{ine}}{V_{ine}(O_{c}^{e}=0)}$

Case $Q = 0$	T _{g,s} (K)	$\tau \frac{\partial Qc}{\partial T}$	E/N (Td) 49.837	(V _i n _e)* m	$\frac{\operatorname{max}\operatorname{Re}(\lambda)}{0}$
$Q_{c}^{c} > 0$ $Q_{c} < 0$	644	0.33	49.844	1.088	69.4
	537	-0.36	49.827	0.874	-38.0

N₂–O₂ mixture at 600 K with or without heat release/absorption are calculated, as shown in figure 2. Clearly the original critical current is decreased by an exother- mic reaction heat release while increased by an endothermic reaction heat absorption.

To further explore the effect of endothermic/exothermic reactions, a detailed comparison is listed for the three cases at the fixed current shown in table 1. The heat addition or absorption alone will shift the reduced electric field, further modify

the ionization term and eventually alter the sign of eigenmodes. By manipulating endothermic/exothermic reactions, the plasma thermal-chemical instability will proceed even at a

moderate discharge power input, at which Joule heating is too weak to trigger the classical thermal-ionization mechanism.

The above analysis is performed in the simplified zerodimensional system. In the realistic reactive plasmas, the Q_c According to equation (25), the sign of the eigenmodes is determined by the competition among different time scales. A temperature-sensitive reaction heat $(Q_c \ 0, \frac{\partial Q_c}{\partial T})$ will not only shift the steady state electron number densities and temperatures, but change the critical current at which $\max[Re(\lambda)] = 0$. The eigenmodes at different current for a

term may originate from various plasma-assisted chemical reactions. For example, low temperature chemistry High Modical carbon fuels may provide the heat source of over 200 W cm $^{-3}$ at the temperature above 600 K [44, 45]. The exothermic reactions include R + $\rm O_2$ $\mbox{\ensuremath{\en$

32 Eigenmodes of different plasma intermediate reaction classes

In molecular plasmas, the thermal-chemical mechanism proceeds through several different plasma reaction classes, which are listed in the mechanism in the supplementary material. Those intermediate plasma reaction classes cut off the direct link between the fluctuation of the electron number density $\delta n_{\rm e}$ and the fluctuation of the translational temperature $\delta T_{\rm g}$. One of the most important intermediate plasma reaction classes in the targeted low-electron-energyregime (\approx eV) is the vibrational excitation and the following vibrational–translational (V–T) relaxation.

As the time scale of the vibrational excitation ($<10^{-10}$ s) is typically much shorter than that of the V–T relaxation (10^{-4} – 10^{-2} s) [16, 46], the thermal-chemical instability becomes more sensitive to V–T relaxation than to the excitation. To consider the role of V–T relaxation on the stabil- ity boundary, equations (11), (14) and (15) are perturbed for the N–O mixture. For simplicity, the V–V energy trans-

fer and heat release are ignored ($\Pi_{VV} = Q_c = Q^V \neq 0$). It is assumed there exists only one higher vibrational energy level and the V–T relaxation process in the mixture proceed as $N_2(\nu)$ N_2 . The characteristic equation for this simplified system is

$$\lambda^{3} + \lambda^{2}(2V_{\text{conc}} + V_{\beta} + V_{\text{VT}})$$

$$= \frac{\partial \hat{V}_{i}}{\partial \hat{V}_{i}}$$

$$+ \lambda \left[V_{\beta}V_{\text{conv}} + (V_{\text{VT}} + V_{\text{conv}})(V_{\beta} + V_{\text{conv}}) - \eta_{\text{T}} \frac{\lambda}{\partial \hat{E}} V_{i}V_{J} \right]$$

$$= \frac{1}{2} \left[V_{\beta}V_{\text{conv}} - \eta_{\text{T}} \frac{\partial \hat{V}_{i}}{\partial \hat{E}} V_{i}V_{J} \right]$$

$$= \frac{1}{2} \left[V_{\text{VT}} + V_{\text{conv}} \right]$$

where $V_{VT} = \frac{1}{r^{VT}}$ is the vibrational–translational energy transfer rate. One limit in equation (26) is $T_{VT} \to i \otimes$, $V_{VT} \to i \otimes$. As T_{VT} is strongly affected by gas temperature, vibrationally-excited species and colliding partners [22, 46], $T_{VT} \to \infty$ corresponds to plasmas with the decreasing of the gas temperature and concentrations of chemically-reactive colliding partners. Under such circumstance the energy pumped into the vibrational level is 'frozen'. Consequently, the critical current is shifted to a larger value to compensate for the energy locked at the vibrational mode. The result is consistent with previous literature [46].

The other limit is the 'equilibrium' V-T relaxation process, i.e. $T_{VT} \rightarrow 0$, or $V_{VT} \rightarrow T_{ben}$ equation (26) is simplified into

$$\tau_{\rm VT}\lambda^3 + \lambda^2 + \lambda(v \text{ conv})$$

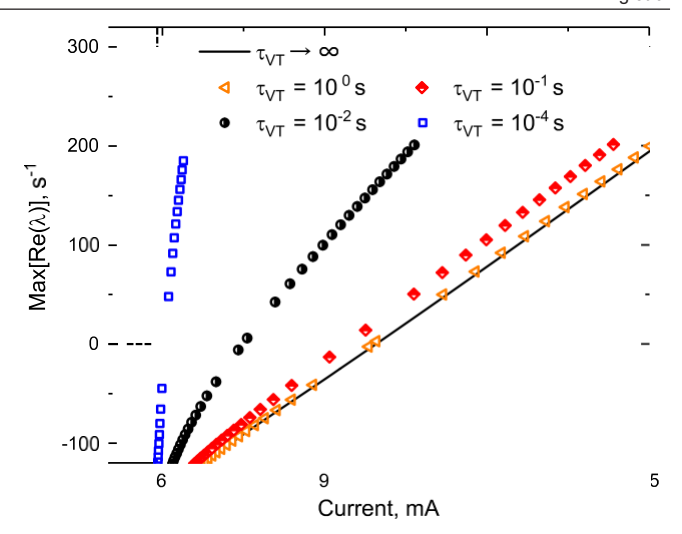


Figure 3. p = 105 Torr. $T_0 = 600$ K. Convective time scale is 1 ms. The maximum eigenvalues at different currents with different vibrational relaxation time scale in the N_2 – O_2 mixture.

This is a typical singular perturbation type of equation. As τ _{VT} approaches zero, the energy transfer from the vibra-tional energy level becomes more dominant. The faster V–T

relaxation destabilizes the system more efficiently and the largest eigenmode crosses zero at a smaller current. Between these two limits (Tinyte rate and Tysically), thermal elemical takes place at a finite rate.

instability in molecular gases will be slowed down because part of Joule heating is first accumulated in vibrational degrees of freedom of molecules. As temperature perturbation grows, $\tau_{\rm VT}$ decreases with temperature and energy stored in the vibrational degree of freedom transforms at an

accelerating rate into the translational energy. The above discussions are validated numerically and plotted in figure 3. Certainly, plasma kinetics of vibrationally excited species are

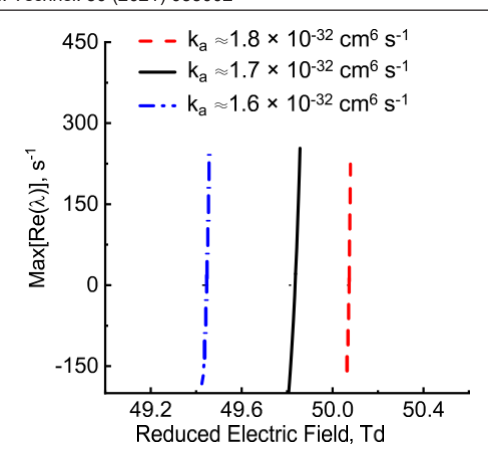
much more complicated than the above simplified model. In the detailed $H_2 - O_2 - N_2$ mechanism, reactions of vibrationally excited species ($H_2(v)$, $O_2(v)$ and $N_2(v)$ are considered, including electron-impact vibrational excitation reactions, vibrational-translational (V-T) relaxation reactions, vibrational-vibrational (V-V) exchange reactions, as well as chemical reactions accelerated by vibrationally excited species. The rate constants of V–T reactions are calculated by using the ordinary method of Schwartz, Slawsky and Herzfeld (SSH theory) and some approximations for the Morse oscillator model [47]. For the V–V reactions between two $H_2(v)$ and $H_2(v)$ molecules, or $O_2(v)$ and $O_2(v)$ molecules, or $N_2(v)$ and $N_2(v)$ molecules, the rate constants are calculated by using the equations described in [47]. The chemical reaction rate constants of vibrationally excited species in overcoming the activation energy barrier are calculated by the Fridman–Macheret *a*-model [46].

$$+ V_{\beta}) +$$

A ons. The charged particle distribution in the con-tracted state no with different attachment rates has been discussed H Zhong et al there.

Plasma Sources Sci. Technol. 30 (2021) 035002 $\frac{1}{\partial} \hat{E}$ $V_{1}V_{J} = 0.$ (27)

ke У in te r m ed iat e pl as m a re ac ti on clas S in th e m ol ec ul ar ga di sc ha rg e is th e el ec tr on att ac h m en t an d de ta ch m en t re ac ti



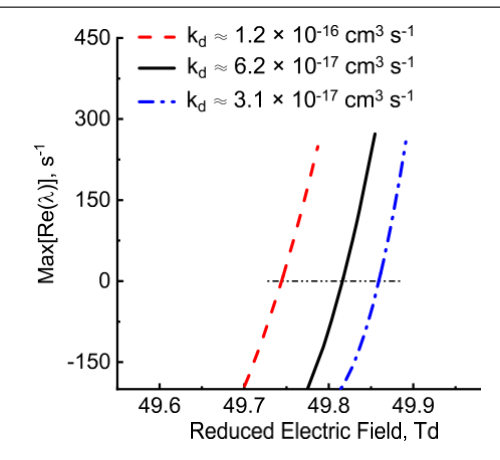


Figure 4. p = 70 Torr. $T_0 = 400$ K. Convective time scale is 1 ms. Left: the maximum eigenvalues at different E/N with different three-body attachment coefficients in N_2 – O_2 mixture. Right: the maximum eigenvalues at different E/N with different detachment coefficients in N_2 – O_2 mixture.

in our previous paper [23]. The impact of electron attachment/detachment reactions on the stability boundary will be analyzed here.

A perturbation of equation (12) at the steady state (i.e., $dn_n/dt = 0$) yields

$$\delta n_{\rm n} = \frac{\overline{\nu}_{\rm a} - \overline{\beta}_{\rm ii} n_{\rm n}}{1/\tau + \overline{\nu}_{\rm d} + \overline{\beta}_{\rm ii} n_{\rm e} + 2\overline{\beta}_{\rm ii} n_{\rm n}} \delta n_{\rm e}. \tag{28}$$

From equation (28), when the system is departed from a steady state, different attachment/detachment rates will affect the balance between electrons and negative ions, and implicitly shift the linear stability of the system. Figure 4 shows the maximum magnitudes of the eigenmodes under different attachment/detachment rates calculated from a simplified N_2 – O_2 system. Stronger electron attachment accelerates the conversion from electrons to ions, making the electron number density, mobility and further Joule heating lower. The stabilization effect shifts the critical reduced electric filed (E/N) to a larger value. In other words, a larger ionization term $V_1(E/N)$ is required for the system to cross the stability boundary. On the contrary, stronger detachment leads to higher electron productions. Extra electrons destabilize the system even when E/N is at a smaller value and ionization rates are at lower levels.

The above discussed V-T relaxation and electron attachment/detachment reactions are representative classes of the intermediate plasma reactions. The analysis is based on the simplified system, but it is helpful for the understanding of the stability in the multi-component chemical system intro-duced in section 3.3, where elementary kinetics lead to a large variation in the composition and temperature. More complicated vibrational reactions are considered and the mixture-averaged attachment/detachment rates vary dramatically with the progress of the kinetics.

3.3. TCMA of elementary kinetics

The analytical stability criterion provides insights of how exothermic/endothermic reactions or specific reaction classes such as V-T relaxation or electron attachment/detachment will influence the stability boundary. They are some important

Table 2. Detailed setup of three cases for the demonstration of the impact of elementary kinetics on the thermal-chemical mechanism.

Case	T_0 (K) p (Torr) I (mA) τ (ms) Initial gas composition							
I	800	200	0.5	5	$N_2:O_2 = 80:20$			
II	800	200	0.5	5	$N_2:O_2:H_2 = 80:6.7:13.3$			
III	825	200	0	5	$N_2:O_2:H_2 = 80:6.7:13.3$			

facets of the thermal-chemical mechanism for the contraction of the plasma volume. However, to further discuss the general effects from chemistry, one has to resort to the detailed chemical kinetic formulation in section (2.1), perform numerical perturbative analysis and reveal chemical modes of a large chemical system with various species and reactions.

In this work, three test cases are compared to demonstrate impact of kinetic coupling between H_2 – O_2 – N_2 ignition chemistry and plasma contraction chemistry on the TCMs [defined in equation (20)] in a plasma-assisted ignition process. The setup of three cases is summarized in table 2. Case I is the normal plasma thermal-ionization instability in air with a limited current input. Case II is the plasma thermal-chemical instability in a stoichiometric N_2 – O_2 – H_2 mixture under the same current. Case III is the homogeneous ignition using the same initial chemical composition as case II. The initial temperature is adjusted purposely from 800 K to 825 K in case III to increase the system reactivity and to make the chemical time scale close to each other [$\mathcal{L}(\mathbf{N})$ ms)] for all three cases.

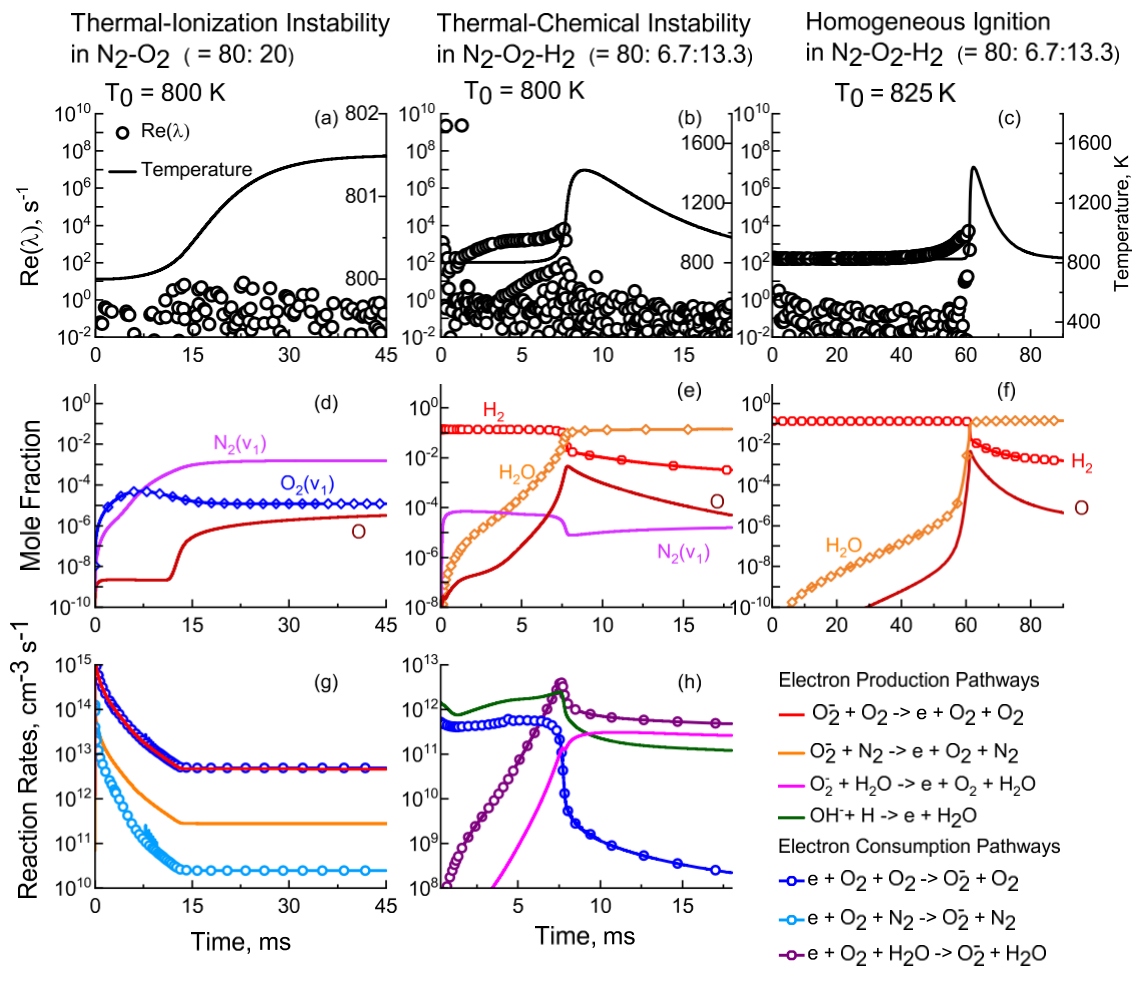


Figure 5. Comparisons among three cases [thermal-ionization instability: (a, d, g), thermal-chemical instability: (b, e, h), homogeneous ignition (c, f)] for the discussion of elementary kinetics. All *x*-axes for (a)–(h) are time in millisecond. Left *y*-axes for (a)–(c) are eigenvalues $Re(\lambda)$ in s^{-1} . Only positive eigenvalues (explosive TCMs) are plotted in the logarithmic scale. Right *y*-axes for (a)–(c) are temperature in K. *Y* -axes for (d)–(f) are mole fractions for active species. *Y* -axes for (g)–(h) are reaction rates of major reactions for the electron production and consumption (in molecule cm⁻³ s⁻¹). Pressure p = 200 Torr. Convective time scale $\tau = 5$ ms. The current for simulating plasma instabilities are I = 0.5 mA.

levels via the V-V energy exchange such as

$$N_2(v = n) + N_2(v = m) \longrightarrow N_2(v = n - 1) + N_2(v = m + 1)$$

$$O(v = n) + O(v = m) \longrightarrow O(v = n - 1) + O(v = m + 1),$$

where m and n indicate the vibrational levels, which are 1-8 for $N_2(v)$ and 1-4 for $O_2(v)$ considered in this study. Reactive radicals such as the atomic oxygen have low number density and are generated either via the electron-impact dissociation reactions such as

$$e + O_2 \longrightarrow e + O + O$$
 (R5)

$$e + O_2 \longrightarrow e + O + O(^1D)$$
 (R6)

or collisional dissociation by electronically excited nitrogen (denoted as N_2^{\ast}) as

$$N_2^* + O_2 \longrightarrow N_2 + O + O(^1D)$$
 (R8)

Atomic oxygen is consumed via ion conversion reactions such as

$$O_2^- + O \longrightarrow O^- + O_2$$
 (R9)

$$O_2^- + O \longrightarrow O_3 + e$$
 (R10)

$$N_2^* + O_2 \longrightarrow N_2 + O + O \tag{R7}$$

from negative oxygen ions O_2^- [shown in figure 5(g)], consistent with the previous studies [20, 21, 23]. Results from case III are plotted in figures 5(c) and (f). The homogeneous ignition in the H_2 – O_2 – N_2 system occurs at approximately 60 ms with the leading positive eigenmodes increasing from ($10^2 \, \mathrm{s}^{-1}$) to ($10^3 \, \mathrm{s}^{-1}$). After the ignition, positive TCMs decay dramatically as the convective heat loss lowers the reactivity and the system converges to the chemical equilibrium.

The distinctive feature of the plasma thermal-chemical instability is the coupling between plasma kinetics and

0 0

Table 3. The list of time (t, unit: ms), largest positive eigenmodes (Re(λ), unit: s⁻¹), the corresponding RAS, and the temperature (T, unit: K) for all three cases.

Case I				Case II				Case III			
t	$\operatorname{Re}(\lambda)$	RAS	T	t	$\operatorname{Re}(\lambda)$	RAS	T	t	$Re(\lambda)$	RAS	T
6	1.4×10^{-2}	NO ₂	800	0.5	2.3×10^{9}	$N_2(v = 6)$	800	6	1.6×10^{2}	О	825
7	1.7×10^{-1}	NO	800	1	1.1×10^{1}	O	800	7	1.6×10^{2}	ОН	825
8	1.6×10^{-1}	N_2O	800	2	4.8×10^{2}	$N_2(v = 8)$	801	16	1.6×10^{2}	HO_2	825
9	1.4×10^{-1}	O	800	3	1.1×10^{3}	$N_2(v=5)$	801	17	1.6×10^{2}	ОН	825
16	3.6×10^{0}	NO	800	5	1.6×10^{3}	$O_2(v = 2)$	803	58	1.8×10^{3}	ОН	825
17	2.1×10^{0}	N	800	6	1.8×10^{3}	$H_2(v = 1)$	810	59	2.4×10^{3}	O	826
18	1.7×10^{0}	$N_2(A)$	800	7	3.2×10^{3}	$H_2(v = 3)$	845	60	2.8×10^{3}	O	834
19	1.6×10^{0}	NO	800	7.5	6.5×10^{3}	N ₂ O	1000	61	6.3×10^{3}	HO_2	993
19.5	1.3×10^{0}	$N_2(A)$	800	8	4.4×10^{1}	H_2O_2	1328	61.2	1.2×10^{3}	H_2	1190
20	1.1×10^{0}	N	800	9	5.1×10^{-1}	H_2O	1420	63	1.3×10^{-3}	О	1422
27	5.1×10^{0}	О	801	15	8.7×10^{-1}	O_2	1080	70	1.2×10^{-3}	O_2	1025
28	1.9×10^{0}	N	801	20	1.2×10^{-1}	N_2	920	75	1.2×10^{-3}	Н	918

combustion kinetics [plotted in figures 5(b), (e) and (h)]. The Joule heating from the discharge provides the initial energy to increase the temperature and 'activates' unstable TCMs of the H_2 – O_2 – N_2 mixture. In figure 5(b), there is a clear growth trend for the magnitude of the TCMs in the initial 7 ms, ranging from 00^{0} s⁻¹) to 00^{4} s⁻¹). This is due to the active energy relaxation from vibrational energies of the excited major species (H₂, N₂, and O₂) to neutral species. Meanwhile, the excited species generated from plasma kinetics interact with each other through reactions like V-V energy exchange and combustion kinetics of the $H_2 - O_2 - N_2$ chemistry, contributing greatly to the gas heating and enhancing the transition from the homogeneous state to the contracted state. At approximately 7 ms, the plasma-assisted ignition occurs with a sharp temperature rise over 400 K and the magnitude of TCMs increases promptly. In addition, new reaction pathways for plasma species are created with the progress of the H₂ -O₂-N₂ chemistry. For example, vibrationally excited nitrogen $N_2(v)$ is deactivated by H radicals and H_2O produced during the ignition process as

$$N_2(v) + H_2O \longrightarrow N_2 + H_2O$$
 (R11)

$$N_2(v) + H \longrightarrow N_2 + H$$
 (R12)

New kinetic pathways are also established for the creation of electrons as

$$OH^- + H \longrightarrow e + H_2O$$
 (R13)

$$O_{2}^{-} + H_{2}O \longrightarrow e + O_{2} + H_{2}O$$
 (R14)

Moreover, although the consumption of electrons is still governed by three-body attachment to oxygen and the formation of oxygen ions, the major collision partners are now switched from N_2 and O_2 in the air case to H_2O in the plasma-assisted ignition case.

From the above analysis, the time-dependent explosive chemical modes differ greatly in the normal thermal-ionization instability (case I) and the thermal-chemical instability (case II) even at the same discharge current input. Chemical kinetics provide new unstable modes to the system. To further understand how TCMs are related to different species, the time-dependent species/temperature pointer (SP) following equation (21) are computed and the RAS for the corresponding eigenmodes are listed in table 3.

In case I, most RAS are related with N_2 – O_2 chemistry and NO_x formation. Those NO_x species including NO_2 , NO and N_2O are in low number densities (below 10^6 cm⁻³) and the corresponding positive TCMs are suppressed to small values. Chemical modes related with excited species like $N_2(A)$ may dominate from time to time. However, their growth rate is too small to trigger the exponential transition from homogeneous state to the unstable state. In other words, all of the unstable modes are not fully activated and the system only goes through a moderate change. In case III, RAS is consistent with previous studies of H_2 – O_2 chemistry [29]. Small radicals including OH, H and O dominate the unstable ignition progress and no excited species are representing or leading the explosive TCMs. In this case only unstable modes from H_2 – O_2 chemistry are fully activated.

Eigenmodes and their RAS are quite different in case II. Before the plasma assisted ignition and dramatic changes in rates of H_2 – O_2 elementary reactions and heat release, TCMs related with small radicals such as O contribute to the destabilization of the plasma system, similar as those in case

III. Moreover, excited species generated from extremely fast plasma kinetics also have significant impact on the unstable modes of the system. For example, vibrationally and electronically excited nitrogen are produced from electron-impact reactions as

$$e + N_2 \longrightarrow e + N_2(v) \tag{R15}$$

$$e + N_2 \longrightarrow e + N_2^*$$
 (R16)

The excited species produced in plasma will further provide reactive radicals to the radical pool to enhance ignition via

$$H_2(v) + OH \longrightarrow H_2O + H$$
 (R17)

$$O_2(v) + H \longrightarrow O + OH$$
 (R18)

$$N_{2}^{*} + O_{2} \longrightarrow N_{2} + O + O/O(^{1}D)/O(^{1}S)$$
 (R19)

$$N_2^* + H_2 \longrightarrow N_2 + H + H$$
 (R20)

The typical concentrations of vibrationally excited species are covering a wide range in magnitudes, from O $(10^{12} \text{ cm}^{-3})$ O $(10^{14} \text{ cm}^{-3})$ for low vibrational levels to O (10^6 cm^{-3}) O (10^8 cm^{-3}) for high vibrational levels. As a result, the magnitudes of the TCMs led by vibrationally excited species can be as large as (10^9 s^{-1}) . For electroni- cally excited species such as $N_2(C)$ and $N_2(a^*)$, even though the typical concentration is below (10^8 cm^{-3}) , the fast quenching relaxation reactions shown above (R19) and (R20) with reaction rates over $(10^{12} \text{ cm}^{-3} \text{ s}^{-1})$ will generate TCMs with growth rates of over 10^4 s^{-1} . At the time of ignition, excited species including $O(^1D)$ and $N_2(\nu)$ continue to accelerate the reaction progress and lead the unstable TCMs

via the aforementioned vibrational-translational excitation and O(¹D) reactions as

$$O(^{1}D) + H_{2} \longrightarrow OH + H$$
 (R21)

$$O(^{1}D) + H_{2}O \longrightarrow OH + OH$$
 (R22)

In this case, TCMs reveal a strong coupling between H_2 – O_2 ignition chemistry, represented by small radicals such as OH or HO_2 with the plasma chemical kinetics, represented by the reactions involving electrons and excited species. What's more, TCMA shows that plasma-generated active species such as N or NNH (related with N_2 – H_2 kinetics), and NO or N_2O (related with N_2 – O_2 kinetics) are involved in the explosive modes as they participate in the energy relaxation process of vibrationally or electronically excited species as

$$N_2(v) + H \longrightarrow NNH$$
 (R23)

$$N_2(v) + O \longrightarrow N + NO$$
 (R24)

$$N_2(A) + O_2 \longrightarrow N_2O + O$$
 (R25)

Those fully-activated unstable modes generalize the original thermal-ionization instability to thermal-chemical instability. Figure 6 visualizes some representative TCMs and the associated major species identified by the SP [defined in equation (21)]. Before the ignition [shown in figure 6(a)], TCMs with large positive eigenvalues are mostly dominated by

vibrationally excited species. The discharge-deposited energy transfers via electrons and different vibrational levels of different species, leading to radical formation and temperature rise. Conventional H_2 – O_2 combustion modes are still present [as 'mode 3' in figure 6(a)], but based on its eigenvalue, this mode with such a small growth rate can hardly trigger the ignition nor the instability in the millisecond time scale alone. Upon the ignition [shown in figure 6(b)], TCMA allows for a clear separation of different modes and provides an overview for reaction dynamics and active species in the thermal-chemical instability. For this case, the dominant mode is still governed by vibrationally-excited plasma-combustion chemistry as $H_2(\nu)$ goes through the chain-branching and energy relaxation reactions as

$$H_2(v = 3) + O \longrightarrow H + OH$$
 (R26)

$$H_2(v = 3) + O \longrightarrow H_2(v = 2) + O$$
 (R27)

The second and third largest modes at $t=7 \times 10^{-3}$ s correspond to the coupling between H_2 – O_2 chemistry and electronically-excited plasma kinetics. Conventional H + OH(+M) $H_2O(+M)$ (M is a third body) still proceeds and the energy relaxation from less-populated electronically excited species still contributes to the dynamics and chemical modes of the system.

In summary, unstable TCMs with multiple time-scales coexist when the thermal-chemical instability is triggered in the presence of elementary kinetics. Plasma kinetics at the sub-millisecond scales boost and couple with the $\rm H_2-O_2-N_2$ kinetics and thus the electron production/consumption pathways are modified greatly. Various excited species are actively involved and interacted in the transition process of the plasma thermal-chemical instability. A systematic method, TCMA, is able to decompose and identify individual TCMs and provides insights of the elementary kinetics of the instability. Future experimental studies are also required to further validate the effect from elementary kinetics on the plasma thermal-chemical instability.

3.4. Stability criterion in the voltage-current characteristic curve

Negative differential conductivity (NDC) in the volt- agecurrent characteristic curve is a major feature of the thermalionization mechanism [48–50]. Previous multi- dimensional simulations [20, 21, 23, 50] already show that there exists a hysteresis transition. In the bistable region shown in figure 7(a), the homogeneous plasma discharge will transit into a contracted state by a strong enough perturbation. With the inclusion of chemical kinetics, how the steady-state voltagecurrent curve will evolve is analyzed in the following content. Due to the limit of zero-dimensional modeling, the focus is the homogeneous ['upper' in figure 7(a)] branch with a high electric field and low electron number density. The contribution from the diffusion in the transition is beyond the scope of this work.

First it is shown that in the non-reactive case the stability boundary in the homogeneous branch has a distinctive

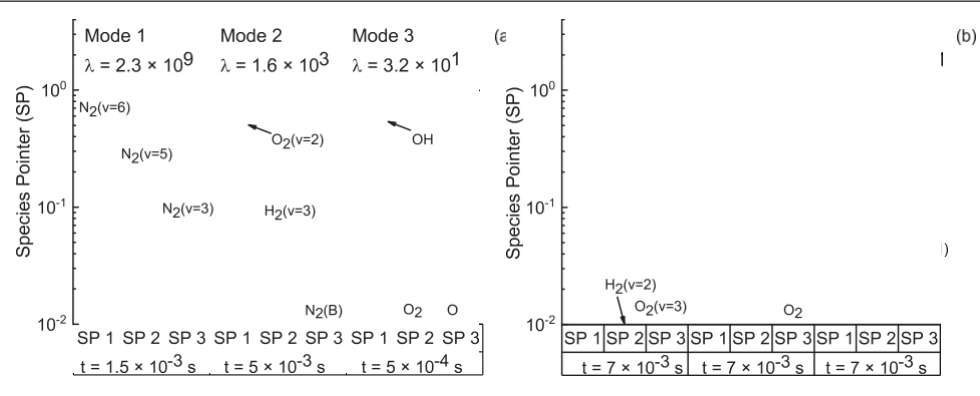


Figure 6. (a) The distributions of SP for three TCMs before the plasma assisted ignition of $H_2 - O_2 - N_2$ system. They are selected from $t = 1.5 \, 10^{-4} \, \text{s}$, $5 \, 10 \, \text{c}^3 \, \text{s}$ and $5 \, 10^{-4} \, \text{s}$ without the loss of generality. For every mode, top three species with their SP values [defined in equation (21)] are visualized. (b) The distributions of SP for three TCMs at the plasma assisted ignition event of $H_2 - O_2 - N_2$ system. The modes are selected from the same time $t = 7 \, 10^{-3} \, \text{s}$, at which the temperature of the system is 845 K. For both (a) and (b), selected modes are displayed in a descending order of the eigenvalues.

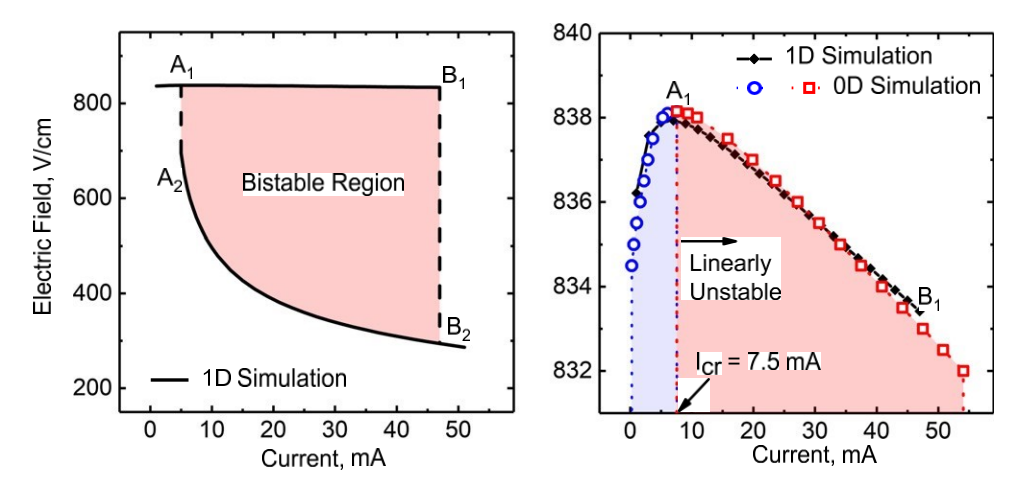


Figure 7. Left: current–voltage characteristics using the one-dimensional simulation in a N_2 – O_2 mixture. The simulation has been reported in [23, 24]. p = 70 Torr and $T_0 = 400$ K. Convective time scale $\tau = 1$ ms. Right: the comparison of the homogeneous branch of the current–voltage characteristics using zero-dimensional and one-dimensional simulation under the same condition. The linearly stable (in blue) and unstable (in red) region are separated by the stability boundary. The critical current in this case is 7.5 mA.

geometrical feature: the bifurcation point as $\max[\text{Re}(\lambda)] = 0$ happens to be the extreme point of the curve E = E(I), i.e. dE/dI = 0. Start from equation (9), dE/dI is expressed as

$$\frac{dE}{dI} = \frac{(dE/d\sigma)}{S \sigma + E dE/d\sigma}$$
(29)

For every steady state, $[dE/d\sigma]_s$ can be derived simply by equating the rhs of equations (11)–(15) to zero. In the simplest case, by considering electro-positive species (negative ion is negligible) without vibrational–translational energy transfer and heat addition ($V_c = 0$), then $[dE/d\sigma]_s = 0$ is equivalent to

$$\frac{\partial \hat{\mathbf{v}}_{i}}{\partial \frac{\hat{E}}{N}} \mathbf{v}_{J} \mathbf{v}_{i} - \mathbf{v}_{\beta} \mathbf{v}_{\text{conv}} = 0 \tag{30}$$

which is exactly the condition when $\lambda = 0$ in the characteristic equation as equation (24). In other words,

$$dE/dI = 0 \Leftrightarrow \max[Re(\lambda)] = 0 \tag{31}$$

This relation could be extended to the case where attachment, vibrational relaxation and heat addition are considered. A validation result of equation (31) is shown in figure 7. The bifurcation point A_1 separates the homogeneous branch into linearly stable and unstable part. This figure also demonstrates the con-

sistency between 0D modeling assumption used in this work and the 1D modeling result reported in our previous paper for small currents. With the increase of the current, in the 1D modeling, a sudden jump occurs at point B_1 and physically represents the transition from the homogeneous state to a contracted state (point B_2). In the 0D modeling, the electric field also keeps dropping with the increase of the current. However, without ambipolar diffusion and other physical

mechanisms, discrepancies appear between those two modeling approaches at larger currents. Future stability analysis in a multi-dimensional modeling framework is still required to further reveal how spatial inhomogeneity will be coupled with unstable thermal-chemical modes.

In the presence of chemical kinetics, the characteristic curve E = E(I) or the slope as dE/dI or $dE/d\sigma$ will be reshaped

by species and reactions. Consider the fully perturbed form of equations (11)–(15) and make several algebraic manipulations (details are revealed in the supplementary material), one can reach the following result as

$$\frac{\delta(\ln \sigma)}{\delta(\ln E)}^{-1} = \frac{1}{\Delta^{t}/\delta(\ln n_{e})|\delta(\ln E)|} + \frac{v_{i,j}\delta x_{j_{-}}}{x_{j}V_{i,j}V_{i,j}^{t}|\delta(\ln E)|} - 1 \qquad (32)$$

$$\times \frac{\delta C - \delta V - \frac{\partial h_j}{\partial T} \omega_j T - h_j \frac{\partial \omega_j}{\partial T} T}{\eta_{\mathrm{T}} \sigma E_{\mathrm{s}}^2} - 2$$

where Δ^t represents interactions between ionization and other plasma kinetics (see supplementary material for more details) and scales linearly with the normalized ionization sensitivity $V_{i,j}^t$ for species j, defined as

$$V_{i,j}^{t} = \frac{\partial V_{i,j}}{\partial (E/N)} / \frac{V_{i,j}}{(E/N)}.$$
 (33)

In other words, Δ^{t} is larger with a larger normalized ionization sensitivity of species j. $V_{i,j}$ is the ionization rate of individual species j. δx_j represents the change of the mass fraction for species j. δC and δV are the cooling term and the energy release term from vibrational relaxation. $\partial h_i/\partial T$ represents the change of the enthalpy for species j with respect to temperature while $\partial \omega_i / \partial T$ represents the change of the total reaction rates for species j with respect to temperature. Equation (32) clearly encodes the original thermal-ionization mechanism. Joule heating $(\eta_T \sigma E_s^2)$, ionization and other plasma kinetics (Δ^t) will influence the differential conductivity. More importantly, chemical kinetics are shown to change the sign of dE/dI and drive the system into the NDC region (dE/dI < 0). The composition update of the mixture ($V_{i,j}\delta x_i$), the change of specific heat for individual species j as $\partial h_i/\partial T$ (con-sistent with previous discussions of ' c_p -controlled plasma' [25, 26]), the change of reaction rates $(\partial \omega_i/\partial T)$ will all contribute to modifying differential conductivity from positive values to negative values.

Physically, when the system is under the NDC region, the filament with a higher local current has a lower electric field. Any departure from the steady states, such as a fluctuation of field, will tend to grow rather than dissipate. Equation (32) clearly shows that NDC is also influenced by different chemical kinetics. The characteristic curve is expected to change dramatically by the thermal-chemical mechanism compared to the classical E = E(I) curve governed only by the thermal-ionization mechanism (shown in figure 7).

4. Conclusion

A general model together with an analytical criterion of plasma thermal-chemical instability is presented for a zerodimensional plasma system. The eigenmodes of the thermalchemical instability involving different plasma energy transfer processes and chemical reaction classes such as vibrational-translational (V-T) relaxation, electron attachment/detachment, and elementary combustion kinetics are investigated. It is shown that the stability criterion or the critical discharge parameter are significantly modified by plasma enhanced reaction kinetics. The TCMA with detailed kinet-

ics is performed in a H_2 – O_2 – N_2 system. It is shown that the explosive mode species/temperature pointer (SP) can successfully identify the important species, defined as 'RAS', and their associated elementary reactions, which contribute greatly to the onset of the instability. The RAS of chemical modes of plasma thermal-chemical instability differ greatly from the

plasma thermal instability and the normal homogeneous ignition. Kinetic pathways including fuel oxidation by vibrational and electronically excited species are shown to be important during the initiation of the 'explosion' of the thermal-chemical modes in the system. Plasma instability and chemical kinetics interact in a variety of time-scales from millisecond to submicrosecond. Moreover, the characteristic current-voltage curve is also reshaped by chemical kinetics. Therefore, understanding the impact of chemical kinetics on plasma instability will provide more insights for the control of plasma instability for various applications from efficient ignition to material synthesis.

Acknowledgments

This work was supported by NSF grant on plasma instabil- ity (NSF CBET-1903362), NSF grant on chemical manufacturing (NSF EFRI DCheM-2029425), DOE grant of Plasma Science Center (DE-SC0020233) and DOE NETL grant (DE-FE0026825). HZ is grateful for support from Eli and Britt Harari Fellowship at Princeton University. HZ also acknowledges the valuable opportunity to discuss CSP with Professor Sau-Hai (Harvey) Lam, a role model, an outstanding mathematician and the founder of CSP theory. The authors also thank Timothy Chen, Tianhan Zhang, Dr. Aric Rousso and Dr. Shuqun Wu at Princeton University for helpful discussions.

ORCID iDs

Hongtao Zhong https://orcid.org/0000-0003-4064-6298 Mikhail N Shneider https://orcid.org/0000-0002-2925-7008

Xingqian Mao https://orcid.org/0000-0003-1042-5144

References

- [1] Smith K and Thomson R M 1978 Computer Modeling of Gas Lasers (Berlin: Springer)
- [2] Nighan W L, Wiegand W J and Haas R A 1973 Ionization instability in CO₂ laser discharges Appl. Phys. Lett. 22 579–82
- [3] Nighan W L and Wiegand W J 1974 Causes of arcing in cw CO₂ convection laser discharges Appl. Phys. Lett. 25 633–6
- [4] Jacob J H and Mani S A 1975 Thermal instability in high-power laser discharges *Appl. Phys. Lett.* **26** 53–5
- [5] Raizer Y P, Milikh G M and Shneider M N 2006 On the mechanism of blue jet formation and propagation *Geophys. Res. Lett.* 33 L23801

- [6] Milikh G M, Shneider M N and Mokrov M S 2014 Model of blue jet formation and propagation in the nonuniform atmosphere J. Geophys. Res. Space Phys. 119 5821–9
- [7] Starikovskiy A and Aleksandrov N 2013 Plasma-assisted ignition and combustion *Prog. Energy Combust. Sci.* 39 61– 110
- [8] Adamovich I V and Lempert W R 2014 Challenges in understanding and predictive model development of plasmaassisted combustion *Plasma Phys. Control. Fusion* 57 014001
- [9] Popov N A 2016 Kinetics of plasma-assisted combustion: effect of non-equilibrium excitation on the ignition and oxidation of combustible mixtures *Plasma Sources Sci. Technol.* 25 043002
- [10] Engelhardt M, Ries S, Hermanns P, Bibinov N and Awakowicz P 2017 Modifications of aluminum film caused by microplasmoids and plasma spots in the effluent of an argon nonequilibrium plasma jet J. Phys. D: Appl. Phys. 50 375201
- [11] Whitehead J C 2016 Plasma-catalysis: the known knowns, the known unknowns and the unknown unknowns J. Phys. D: Appl. Phys. 49 243001
- [12] Sobiecki J R, Wierzchon T, Karpinski T and Rudnicki J 2000 Modification of the microstructure and properties of Ti– 1Al–1Mn titanium alloy due to nitriding and oxynitriding under glow discharge conditions Fourth Institute of Materials Int. Conf. on the Microstructure of High Temperature Materials: Microstructure and Properties of Titanium Alloys pp 229–35
- [13] Choi I, Uddi M, Jiang N, Adamovich I and Lempert W 2009 Stability and heating rate of air and ethylene-air plasmas sustained by repetitive nanosecond pulses 47th AIAA Aerospace Sciences Meeting p 688
- [14] Kerner B S and Osipov V V 1989 Sov. Phys. Usp. 32 101
- [15] Ecker G, Kro"ll W and Zo"ller O 1964 Thermal instability of the plasma column *Phys. Fluids* **7** 2001–6
- [16] Haas R A 1973 Plasma stability of electric discharges in molecular gases Phys. Rev. A 8 1017
- [17] Allis W P 1976 Review of glow discharge instabilities *Physica* B **82** 43–51
- [18] Velikhov E P, Golubev V S and Pashkin S V 1982 Glow discharge in a gas flow Sov. Phys. Usp. 25 340
- [19] Golubovskii Y B, Nekuchaev V, Gorchakov S and Uhrlandt D 2011 Contraction of the positive column of discharges in noble gases *Plasma Sources Sci. Technol.* 20 053002
- [20] Shneider M N, Mokrov M S and Milikh G M 2012 Dynamic contraction of the positive column of a self- sustained glow discharge in molecular gas *Phys. Plasmas* 19 033512
- [21] Shneider M N, Mokrov M S and Milikh G M 2014 Dynamic contraction of the positive column of a self-sustained glow discharge in air flow *Phys. Plasmas* 21 032122
- [22] Raizer Y P 1991 Gas Discharge Physics (Berlin: Springer)
- [23] Zhong H, Shneider M N, Mokrov M S and Ju Y 2019 Thermalchemical instability of weakly ionized plasma in a reactive flow J. Phys. D: Appl. Phys. 52 484001
- [24] Zhong H, Shneider M N, Mokrov M S and Ju Y 2020 Thermalchemical plasma instability in a reacting flow *AIAA Scitech* 2020 Forum p 1661
- [25] Wolf A J, Righart T W H, Peeters F J J, Bongers W A and van de Sanden M C M 2020 Implications of thermochemical instability on the contracted modes in CO₂ microwave plasmas Plasma Sources Sci. Technol. 29 025005
- [26] Viegas P, Vialetto L, Wolf A J, Peeters F, C Groen P W, Righart T H, Bongers W, Van de Sanden R and Diomede P 2020 Insight into contraction dynamics of microwave plasmas for CO₂ conversion from plasma chemistry modelling *Plasma Sources Sci. Technol.* 29 105014

- [27] Rousso A C, Goldberg B M, Chen T Y, Wu S, Dogariu A, Miles R B, Kolemen E and Ju Y 2020 Time and space resolved diagnostics for plasma thermal-chemical instability of fuel oxidation in nanosecond plasma discharges *Plasma Sources* Sci. Technol. 29 105012
- [28] Golubovskii Y, Valin S, Pelyukhova E and Nekuchaev V 2019 Instabilities of a constricted gas discharge with respect to two-dimensional wave perturbations *Plasma Sources Sci.* Technol. 28 045015
- [29] Lam S H and Goussis D A 1989 Understanding complex chemical kinetics with computational singular perturbation *Symp.* (*Int.*) on Combustion (Elsevier) 22 931–41
- [30] Lu T F, Yoo C S, Chen J H and Law C K 2010 Threedimensional direct numerical simulation of a turbulent lifted hydrogen jet flame in heated coflow: a chemical explosive mode analysis *J. Fluid Mech.* 652 45
- [31] Douglas-Hamilton D H and Mani S A 1973 An electron attachment plasma instability Appl. Phys. Lett. 23 508–10
- [32] Flitti A and Pancheshnyi S 2009 Gas heating in fast pulsed discharges in N₂ –O₂ mixtures Eur. Phys. J. Appl. Phys. 45 21001
- [33] Mao X, Chen Q, Rousso A C, Chen T Y and Ju Y 2019 Effects of controlled non-equilibrium excitation on H2/O2/He ignition using a hybrid repetitive nanosecond and DC discharge Combust. Flame 206 522–35
- [34] Pancheshnyi S, Eismann B, Hagelaar G J M and Pitchford L C 2008 Computer Code Zdplaskin (Toulouse, France: University of Toulouse, LAPLACE, CNRS-UPS-INP)
- [35] Lutz A E, Kee R J and Senkin J A M 1988 A fortran program for predicting homogeneous gas phase chemical kinetics with sensitivity analysis *Technical Report* (Livermore, CA USA: Sandia National Labs)
- [36] Mao X, Rousso A, Chen Q and Ju Y 2019 Numerical modeling of ignition enhancement of CH₄/O₂/He mixtures using a hybrid repetitive nanosecond and dc discharge *Proc. Com*bust. Inst. 37 5545–52
- [37] Zhong H, Mao X, Rousso A C, Patrick C L, Yan C, Xu W, Chen Q, Wysocki G and Ju Y 2020 Kinetic study of plasmaassisted n-dodecane/O₂/N₂ pyrolysis and oxidation in a nanosecond-pulsed discharge *Proc. Combust. Inst.* https:// doi.org/10.1016/j.proci.2020.07.095
- [38] Hagelaar G J M and Pitchford L C 2005 Solving the Boltzmann equation to obtain electron transport coefficients and rate coefficients for fluid models *Plasma Sources Sci. Technol.* 14 722
- [39] Pancheshnyi S, Biagi S, Bordage M C, Hagelaar G J M, Morgan W L, Phelps A V and Pitchford L C 2012 The lxcat project: electron scattering cross sections and swarm parameters for low temperature plasma modeling *Chem. Phys.* 398 148–53
- [40] Yang X, Shen X, Santner J, Zhao H and Ju Y 2017 Princeton hp-mech. URL http://engine.princeton.edu/mechanism/HP-Mech.html
- [41] Garscadden A and Nagpal R 1995 Non-equilibrium electronic and vibrational kinetics in H₂–N₂ and H₂ discharges *Plasma Sources Sci. Technol.* **4** 268
- [42] Guerra V, Tejero-del-Caz A, Pintassilgo C D and Alves L L 2019 Modelling N₂-O₂ plasmas: volume and surface kinetics Plasma Sources Sci. Technol. 28 073001
- [43] Gutsol A, Rabinovich A and Fridman A 2011 Combustionassisted plasma in fuel conversion J. Phys. D: Appl. Phys. 44 274001
- [44] Reuter C B, Won S H and Ju Y 2016 Experimental study of the dynamics and structure of self-sustaining premixed cool flames using a counterflow burner *Combust. Flame* 166 125– 32
- [45] Ju Y, Reuter C B, Yehia O R, Farouk T I and Won S H 2019 Dynamics of cool flames Prog. Energy Combust. Sci. 75 100787

- [46] Fridman A 2008 *Plasma Chemistry* (Cambridge: Cambridge University Press)
- [47] Capitelli M, Ferreira C M, Gordiets B F and Osipov A I 2013 Plasma Kinetics in Atmospheric Gases vol 31 (Berlin: Springer)
- [48] Vedenov A A, Gladush G G, Griukanova L G and Samokhin A A 1980 Voltage-current characteristics of a diffusion-sustained glow discharge in a flowing gas Sov. J. Plasma Phys. 6 499– 504
- [49] Almeida P G C, Benilov M S, Cunha M D and Faria M J 2009
 Analysing bifurcations encountered in numerical modelling of current transfer to cathodes of dc glow and arc discharges *J. Phys. D: Appl. Phys.* 42 194010
- [50] Shkurenkov I A, Mankelevich Y A and Rakhimova T V 2009 Simulation of diffuse, constricted-stratified, and constricted modes of a dc discharge in argon: hysteresis transition between diffuse and constricted-stratified modes *Physical Review* E 79 046406